



Decoupling or Learning: Joint Power Splitting and Allocation in MC-NOMA With SWIPT

Journal:	<i>IEEE Transactions on Communications</i>
Manuscript ID	TCOM-TPS-19-1172.R1
Manuscript Type:	Transactions Paper Submissions
Date Submitted by the Author:	10-Feb-2020
Complete List of Authors:	Tang, Jie; South China University of Technology, School of Electronic and Information Engineering Luo, Jinci; South China University of Technology, School of Electronic and Information Engineering Ou, Junhui; South China University of Technology, School of Electronic and Information Engineering Zhang, Xiu Yin; South China University of Technology, School of Electronic and Information Engineering Zhao, Nan; Dalian University of Technology, School of Information and Communication Engineering So, Daniel Ka Chun; University of Manchester, School of Electrical & Electronics Engineering Wong, Kai Kit; University College London, Electronic and Electrical Engineering
Keyword:	Communication, Communication systems, Resource management

SCHOLARONE™
Manuscripts

Decoupling or Learning: Joint Power Splitting and Allocation in MC-NOMA With SWIPT

Jie Tang, *Senior Member, IEEE*, Jingci Luo, Junhui Ou, *Member, IEEE*
 Xiuyin Zhang, *Senior Member, IEEE*, Nan Zhao, *Senior Member, IEEE*,
 Daniel Ka Chun So, *Senior Member, IEEE*, Kai-Kit Wong, *Fellow, IEEE*

Abstract—Non-orthogonal multiple access (NOMA) is one of the most significant technologies to meet the demand of high spectral efficiency (SE) in the fifth generation (5G) cellular networks. The utilization of simultaneous wireless information and power transfer (SWIPT) contributes to prolonging the battery life of the mobile users (MUs) and enhancing the system energy efficiency (EE), especially in the NOMA scenario where the multi-user interference can be reused for energy harvesting (EH). In this paper, we study the achievable data rate maximization problem for the downlink multi-carrier NOMA (MC-NOMA) network with power splitting (PS)-based SWIPT, in which power allocation and PS control are jointly optimized with the limitation of available power budget as well as the requirement for EH. The considered non-convex optimization problem is arduous to tackle, resulting from the presence of the coupled variables and the multi-user interference. To cope with the problem, a decoupled approach is developed, in which the power allocation and PS control are separated and the corresponding sub-problems are respectively solved through Lagrangian duality method. Furthermore, an alternative approach based on deep learning is proposed, which is capable of effectively obtaining the approximate optimal solution according to the empirical data. Simulation results confirm the effectiveness of the proposed schemes, and demonstrate the superiority of the combination of PS-based SWIPT with MC-NOMA over SWIPT-aided single-carrier NOMA (SC-NOMA) and SWIPT-aided orthogonal multiple access (OMA).

Index Terms—Multi-carrier non-orthogonal multiple access (MC-NOMA), simultaneous wireless information and power transfer (SWIPT), deep learning.

I. INTRODUCTION

With the exponential expansion of terminal equipments and the increasing popularity of the wireless application scenarios such as Internet of Things (IoT) and massive machine-type communications (mMTC) [1], the booming fifth generation (5G) wireless communication networks are increasingly required to supply services with much higher quality, including higher data rate, lower latency, greater reliability and larger connectivity. The non-orthogonal multiple access (NOMA) scheme has been regarded as an irreplaceable technique for future communication system to satisfy the aforementioned demands [2], [3], due to its capability of enabling multiple mobile users (MUs) to receive signals from the base station (BS) through the same radio frequency (RF) channel. Compared to those traditional orthogonal multiple access (OMA) transmission schemes, the channel orthogonality elimination enables the NOMA system to provide a considerably better spectrum efficiency (SE). Nevertheless, the co-channel interference caused by non-orthogonality hinders the further

improvement of SE to some extent. Hence, successive interference cancellation (SIC) [4] is always employed in the receiving ends of NOMA system to estimate the co-channel interference, resulting in a much higher SE [5]. Based on this observation, NOMA technique has attracted considerable attention and the system-level performance superiority to the conventional OMA has been confirmed. In [6], the downlink of NOMA system with randomly distributed MUs was investigated, and the results proved that NOMA outperformed OMA with regard to the ergodic sum rates. In [7], the authors showed that a great performance gain of achievable data rate of the system compared to OMA system could be achieved in NOMA scenario for both macro-cell and small-cell deployments. Similar results for the performance of achievable data rate and power efficiency of the system could also be found in [8] and [9] respectively for multiple-input single-output (MISO) NOMA network. Furthermore, the application of NOMA to other advanced techniques has also been investigated, including multiple-input multiple-output (MIMO) [10], cognitive radio [11], multi-point cooperative relaying [12], [13], etc..

In addition to guaranteeing the requirements of high data rate, low latency and ultra reliability, how to enhance the endurance of numerous power-limited mobile devices is also a significant matter in 5G networks, especially in the application scenarios of IoT and mMTC. Motivated by the emergence as well as the progress of wireless power transfer (WPT) [14], a novel technique called simultaneous wireless information and power transfer (SWIPT) was proposed in [15], which made it possible to collect energy and receive information at the same time. Nevertheless, the difference in signal sensitivity between the information decoder and the rectifier circuit hinders the application and promotion of SWIPT technology. To overcome this difficulty, two practical receiving schemes, time switching (TS) and power splitting (PS), were proposed in [16], where information decoding (ID) and energy harvesting (EH) were performed in different time domains and power domains, respectively. Since part of RF signal is collected for powering the mobile terminals, SWIPT makes it possible to improve the system energy efficiency (EE) and hence is regarded as a promising green communication solution for future wireless networks [14]. Therefore, it has attracted attention in both academic and industry [17]–[21]. Liang *et al.* in [18] investigated the optimal PS solution to attain the “rate-energy (R-E)” region for the single-input single-output (SISO) system with SWIPT, and further expanded the optimal PS solution to the SWIPT-based single-input multiple-

output (SIMO) system. The signal-to-interference-plus-noise ratio (SINR)-constrained and EH-constrained transmit power minimization problem was studied in [19] for the multiple-input single-output (MISO) downlink scenario with SWIPT, in which the transmit beamforming as well as the receive PS control was jointly optimized. In [20], the optimal dual-layer solution for joint resource allocation was proposed to achieve the maximum EE for the MIMO broadcast channel with TS-based SWIPT, in which the maximum transmit power supply was limited and the demand for quality-of-service (QoS) was considered. In addition, SWIPT was also studied in various multiple access schemes. In [21], SWIPT was applied both in time division multiple access (TDMA)-based and orthogonal frequency division multiple access (OFDMA)-based schemes, aiming at maximizing the achievable data rate of the system through dealing with the transmit power allocation and the TS/PS control jointly. The results suggested that both SWIPT-enabled TDMA and SWIPT-enabled OFDMA outperformed the conventional ones in terms of achievable data rate of the system. Besides, there are also many studies in the existing literature on the application of SWIPT to the spectrum-efficient NOMA systems [22]–[24].

A. Contributions

Previous literatures in [22]–[24] evaluated the system performance of SWIPT-enabled NOMA system and confirmed that the advantages of NOMA compared with OMA existed in the system of SWIPT application. Nevertheless, most of the existing studies focused on the single-carrier NOMA (SC-NOMA) systems. On the other hand, the multi-carrier waveform is considered to be the key characteristic in 5G. The work in [25] addressed the achievable data rate maximization problem in the downlink multi-carrier NOMA (MC-NOMA) network and demonstrated that the considered system achieved a remarkable performance improvement contrasted to the traditional SC-NOMA system. **However, the complexity of SIC in MC-NOMA system is significantly higher than that in SC-NOMA, especially for large number of users in practical 5G communication application scenarios, which is the main challenge in using MC-NOMA over SC-NOMA. In addition, the performance of the application of SWIPT to MC-NOMA scenario is still an open topic. Inspired by this, we consider a novel system which combines the spectrum-efficient MC-NOMA and energy-efficient SWIPT.**

Moreover, deep learning method, which has been widely applied in various fields, is recently utilized for solving the problems in the field of communication, such as route estimation [26], mobility forecast [27], resource allocation [28], etc.. Driven by the aforementioned studies, we develop an alternative approach by applying deep learning to acquire the approximated optimal solution to the intricate problem, which achieves a balance between the optimality and the demand for low latency. The main contributions of this work are summarized as follows:

- We investigate a novel scenario where the PS-SWIPT is applied in the MC-NOMA system. The joint power allocation and splitting control problem is mathematically

modelled to maximize the achievable data rate of the system with the constraints of transmit power and EH requirement. The presence of the coupled variables and the intra-interference lead to the non-convex and intricate problem. To tackle this problem, two approaches are developed.

- In the first proposed approach, we decouple the two variables, i.e., transmit power and PS ratios, and develop a dual-layer iterative method. We first solve the sub-problem of optimizing PS ratio assignment under fixed power allocation; then we turn to determine the optimal solution of power allocation with given PS ratio. Both the sub-problems are solved by applying the Lagrangian duality method. This procedure is repeated until convergence.
- An alternative approach based on deep learning is then proposed to achieve the approximation of the optimal solution to the optimization problem. Specifically, the general deep belief network (DBN) model is adopted and the learning-based approach involves three phases, i.e., data preparation, training and running.
- The effectiveness and superiority of our developed approaches are validated. More importantly, numerical results indicate that the considered PS-based MC-NOMA system outperforms the existing wireless scenarios in terms of achievable data rate, including PS-based SC-NOMA system and PS-based OMA system.

B. Organization

The remainder of this paper is arranged as follows. In Section II, the system model of MC-NOMA with PS-based SWIPT is provided and the corresponding power-limited and QoS-constrained achievable data rate maximization problem is modelled mathematically. In Section III, a dual-layer iterative strategy for joint transmit power allocation and PS control is developed to solve the problem. Furthermore, an alternative learning-based algorithm is proposed in Section IV. Lastly, simulations and conclusions are respectively given in Section V and Section VI.

Notation: The lower- and upper-case boldface letters denote column vectors and matrixes, respectively. $\mathbb{E}[|x|^2]$ and $[x]^T$ denote the energy and the transposition of x , respectively. $\mathcal{CN}(0, \sigma^2)$ represents the complex Gaussian random variable with zero mean and the variance of σ^2 .

II. SYSTEM MODEL AND PROBLEM FORMULATION

In this section, we firstly describe the system model of the considered MC-NOMA with PS-based SWIPT, and then mathematically modelled the power-limited and QoS-constrained achievable data rate maximization problem.

A. System Model

The considered downlink SWIPT-enabled MC-NOMA system is presented in Fig. 1, in which a single antenna BS provides service for K MUs through N subcarriers. All the transceivers are equipped with a single antenna. Let

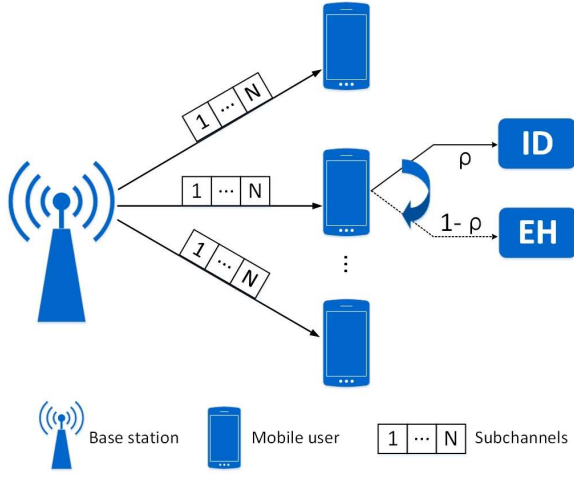


Fig. 1: The system model of the downlink SWIPT-aided MC-NOMA with PS-based receivers.

$\mathcal{K} = \{1, 2, \dots, K\}$ and $\mathcal{N} = \{1, 2, \dots, N\}$ represent the set of MUs' indexes and the set of subchannels' indexes, respectively. The available bandwidth for the proposed system is BW and it is allocated to N orthogonal subcarriers with the equal value of $BW_n = BW/N$. It is worth noting that the transmission signals over any two subcarriers will not cause interference to each other, owing to the setting of channel orthogonality. Therefore, the observation in the k -th MU on the n -th subchannel is given by

$$y_{n,k} = h_{n,k} \left(\sqrt{p_{n,k}} s_{n,k} + \sum_{j \in \mathcal{K}, j \neq k} \sqrt{p_{n,j}} s_{n,j} \right) + z_{n,k}, \quad (1)$$

where $h_{n,k}$ denotes the channel gain between the transmitter and the k -th MU on the n -th subcarrier; $p_{n,k}$ ($p_{n,j}$) represents the transmit power allocated to the k -th (j -th) MU over the n -th subchannel; $s_{n,k}$ ($s_{n,j}$) denotes the transmitted data symbol from the BS to the k -th (j -th) MU over the n -th subchannel, which is an independent and identically distributed (i.i.d) circularly symmetric complex Gaussian (CSCG) random signal with zero mean and unit variance, i.e., $\mathbb{E}[|s_{n,k}|^2] (\mathbb{E}[|s_{n,j}|^2]) = 1$; $z_{n,k} \sim \mathcal{CN}(0, |\sigma_{n,k}|^2)$ refers to the additive white Gaussian noise (AWGN) to the k -th MU on the n -th subcarrier.

For the PS-based SWIPT setup, all the MUs are considered as the combination of an information decoder and a rectifier circuit. The received signal of each MU is divided into two parts by a PS mechanism. More specifically, for the k -th MU, the PS ratio $\sqrt{\rho_k}$ and $\sqrt{1-\rho_k}$ are the proportions of the received signal for ID and EH, respectively. Accordingly, the received signal for EH and ID are respectively given by

$$y_{n,k}^{\text{EH}} = h_{n,k} \sum_{j=1}^K \sqrt{(1-\rho_j) p_{n,j}} s_{n,j} + \sqrt{1-\rho_k} z_{n,k}, \quad (2)$$

and

$$y_{n,k}^{\text{ID}} = \underbrace{h_{n,k} \sqrt{\rho_k p_{n,k}} s_{n,k}}_{\text{Intended signal}} + \underbrace{h_{n,k} \sum_{\substack{j \in \mathcal{K}, \\ j \neq k}} \sqrt{\rho_k p_{n,j}} s_{n,j}}_{\text{Interference signal}} + \underbrace{\sqrt{\rho_k} z_{n,k} + z_{n,k}^{\text{ID}}}_{\text{Noise}}, \quad (3)$$

where $z_{n,k}^{\text{ID}} \sim \mathcal{CN}(0, |\sigma_{n,k}^{\text{ID}}|^2)$ corresponds to the additional noise generated during power splitting.

The SIC technique is utilized by the information receivers to mitigate the interference when decoding information. Denote $\tilde{h}_{n,k} = |h_{n,k}|^2 / |\sigma_{n,k}|^2$ as the channel to noise ratio (CNR) for the k -th MU over the n -th subcarrier. In general, the decoding order in the downlink NOMA system is always consistent with the increasing order of the CNR. Thereby, the interference for the k -th MU on the n -th subcarrier is given by

$$I_{n,k} = \rho_k |h_{n,k}|^2 \sum_{\substack{j \in \mathcal{K}, \\ \tilde{h}_{n,j} > \tilde{h}_{n,k}}} p_{n,j}. \quad (4)$$

Therefore, the SINR of the k -th MU on the n -th subcarrier is formulated as

$$\text{SINR}_{n,k} = \frac{|h_{n,k}|^2 \rho_k p_{n,k}}{I_{n,k} + \rho_k |\sigma_{n,k}|^2 + |\sigma_{n,k}^{\text{ID}}|^2}. \quad (5)$$

Furthermore, the available data rate of the k -th MU on the n -th subcarrier is given by

$$R_{n,k} = BW_n \log_2(1 + \text{SINR}_{n,k}). \quad (6)$$

On the other hand, the energy collected by the EH receiver at the k -th MU on the n -th subcarrier can be modelled as

$$E_{n,k} = \eta(1 - \rho_k) \left(|h_{n,k}|^2 \sum_{j=1}^K p_{n,j} + |\sigma_{n,k}|^2 \right), \quad (7)$$

where η indicates the loss of the EH circuits for transferring the received signal into battery energy.

Thus, the achievable data rate and energy for the k -th MU are respectively given by

$$R_k = \sum_{n=1}^N R_{n,k}, \quad (8)$$

$$E_k = \sum_{n=1}^N E_{n,k}. \quad (9)$$

Accordingly, we can express the achievable data rate of the considered SWIPT-enabled MC-NOMA system as

$$R_{\text{sum}} = \sum_{n=1}^N \sum_{k=1}^K R_{n,k} = \sum_{k=1}^K R_k. \quad (10)$$

B. Problem Statement

In this paper, we intend to obtain the maximum achievable data rate of the PS-SWIPT aided MC-NOMA system by jointly optimizing the power allocation and the PS control, whilst satisfying the desired EH constraints and the transmit

power limitation. Thus, the considered achievable data rate maximization problem can be mathematically formulated as follows

$$\max_{\boldsymbol{\rho}, \mathbf{p}} R_{\text{sum}}(\boldsymbol{\rho}, \mathbf{p}) \quad (11)$$

$$\text{s.t.} \quad E_k \geq E_{\text{req}}, \quad \forall k \in \mathcal{K}, \quad (12)$$

$$0 < \rho_k < 1, \quad \forall k \in \mathcal{K}, \quad (13)$$

$$p_{n,k} \geq 0, \quad \forall n \in \mathcal{N}, \quad \forall k \in \mathcal{K}, \quad (14)$$

$$\sum_{n=1}^N p_{n,k} \leq p_k^{\text{max}}, \quad \forall k \in \mathcal{K}, \quad (15)$$

where $\boldsymbol{\rho} = [\rho_1, \rho_2, \dots, \rho_K]^T$ and $\mathbf{p} = [\mathbf{p}_1, \mathbf{p}_2, \dots, \mathbf{p}_N]^T$ with the component $\mathbf{p}_n = [p_{n,1}, p_{n,2}, \dots, p_{n,K}]^T$ ($1 \leq n \leq N$). The constraint (12) indicates that each MU is required to collect at least E_{req} energy. The constraint (13) limits the PS ratio for each MU to be in the range of $(0, 1)$. The constraint (14) guarantees the non-negativity of the power allocated to the k -th MU on the n -th subcarrier. Constraint (15) defines that the total power allocated to the k -th MU, i.e., $\sum_{n=1}^N p_{n,k}$, can not exceed the threshold of p_k^{max} , which guarantees the MUs' proportional fairness to some extent [29]. Besides, the maximum total transmission power of the BS can be implied from the constraint (15), i.e., $\sum_{k=1}^K p_k^{\text{max}}$.

The achievable data rate maximization problem formulated in (11)-(15) is neither convex nor linear as the result of the coupling of multiple variables and the presence of multi-user interference [30]. Additionally, the aforementioned maximization problem is a widely-known NP-hard problem, and hence the solution is complicated and can not be obtained directly. The exhaustive search method by traversing all possible power allocation and PS ratio assignment might be one of the solutions to this problem. However, the computational complexity of the exhaustive search method will mount dramatically as the number of MUs or subcarriers grows. Consequently, this method is far from practical, especially for the IoT scenario with the demand for massive connections. In the following sections, based on the Lagrangian duality theory and deep learning technique, we propose two different approaches to tackle the problem in (11)-(15).

III. ALGORITHM BASED ON LAGRANGIAN DUALITY

In this section, we develop the power allocation and PS control strategy for the involved PS-SWIPT aided MC-NOMA system. Since the coupled variables $\boldsymbol{\rho}$ and \mathbf{p} make the original problem (11)-(15) non-convex, it is extremely tough to derive the optimal solution directly. According to [31], for any optimization problem involving multiple variables, it is practicable to deal with the sub-problem over part of variables while considering the remainder as constants, and next turn to handle the sub-problem over the remaining variables. As a result, \mathbf{p} and $\boldsymbol{\rho}$ are separated to develop the practical and effective solution for the considered optimization problem.

A. PS Control With Fixed Power Allocation

We first consider the case where all the components of the power allocation matrix \mathbf{p} are constants. In this case, we focus

on optimizing the PS ratios under the fixed power allocation. Hence, the corresponding sub-problem can be simplified as

$$\max_{\boldsymbol{\rho}} R_{\text{sum}}(\boldsymbol{\rho}) \quad (16)$$

$$\text{s.t.} \quad 0 < \rho_k < 1, \quad \forall k \in \mathcal{K}, \quad (17)$$

$$E_k \geq E_{\text{req}}, \quad \forall k \in \mathcal{K}. \quad (18)$$

According to (7), (9) and (18), ρ_k ($\forall k \in \mathcal{K}$) is required to satisfy the following condition

$$\rho_k \leq 1 - \frac{E_{\text{req}}}{\eta \sum_{n=1}^N |h_{n,k}|^2 \sum_{j=1}^K p_{n,j} + |\sigma_{n,k}|^2} \triangleq \rho_k^{\text{UB}}. \quad (19)$$

Considering (17) and (19) together, the optimization problem (16)-(18) is infeasible unless

$$\rho_k^{\text{UB}} > 0, \quad \forall k \in \mathcal{K}. \quad (20)$$

Proposition 1: Suppose that the process of PS in the receiving ends is almost idealized and the noise power for all MUs on the n -th subchannel is equal, i.e., $|\sigma_{n,k}^{\text{ID}}|^2 \rightarrow 0$ and $|\sigma_{n,k}|^2 = |\sigma_{n,j}|^2 = |\sigma_n|^2$ ($\forall k, j \in \mathcal{K}$). Under the fixed power allocation $\bar{\mathbf{p}}$ satisfying (14), (15) and (20), the sub-problem given in (16)-(18) is convex with regard to $\boldsymbol{\rho}$.

Proof: Please refer to Appendix A. ■

Consequently, it is possible to obtain the near-optimal solution to (16)-(18) by employing the Lagrangian duality based method [31]. The corresponding Lagrangian function is formulated as (21) on the top of the next page, in which $\boldsymbol{\mu} = [\mu_1, \dots, \mu_K]^T$, $\boldsymbol{\nu} = [\nu_1, \dots, \nu_K]^T$ and $\boldsymbol{\omega} = [\omega_1, \dots, \omega_K]^T$ are non-negative Lagrange multipliers, and $C_{n,k}$ is concretely defined as equation (60) in Appendix A. More specifically, $\boldsymbol{\mu}$ and $\boldsymbol{\nu}$ are corresponding to the constraint (17) while $\boldsymbol{\omega}$ is pertaining to the constraint (18).

Then the Lagrange dual objective function can be accordingly written as

$$g(\boldsymbol{\mu}, \boldsymbol{\nu}, \boldsymbol{\omega}) = \max_{\boldsymbol{\rho}} \mathcal{L}(\boldsymbol{\rho}, \boldsymbol{\mu}, \boldsymbol{\nu}, \boldsymbol{\omega}). \quad (22)$$

Thus, the Lagrange dual problem can be modelled as follows

$$\min_{\boldsymbol{\mu}, \boldsymbol{\nu}, \boldsymbol{\omega}} g(\boldsymbol{\mu}, \boldsymbol{\nu}, \boldsymbol{\omega}) \quad (23)$$

$$\text{s.t.} \quad \boldsymbol{\mu} \succeq \mathbf{0}, \boldsymbol{\nu} \succeq \mathbf{0}, \boldsymbol{\omega} \succeq \mathbf{0}. \quad (24)$$

To solve the Lagrange dual problem, we first optimize the PS ratio $\boldsymbol{\rho}$ with the given dual variables $\{\boldsymbol{\mu}, \boldsymbol{\nu}, \boldsymbol{\omega}\}$ through gradient ascent method, and then update the dual variables $\{\boldsymbol{\mu}, \boldsymbol{\nu}, \boldsymbol{\omega}\}$ with the optimized $\boldsymbol{\rho}$ through well-known sub-gradient scheme [32].

1) *Optimizing $\boldsymbol{\rho}$ With Given Dual Variables $\{\boldsymbol{\mu}, \boldsymbol{\nu}, \boldsymbol{\omega}\}$:* We first calculate the gradient direction of the Lagrangian function (21) regarding the PS ratio ρ_k ($\forall k \in \mathcal{K}$), which is given by (25) at the top of the next page, where $A_{n,k}$, $B_{n,k}$ and $C_{n,k}$ are respectively defined as (58), (59) and (60) in Appendix A.

Particularly, ρ_k can be sequentially updated according to the following formula

$$\rho_k(n+1) = \rho_k(n) + \varepsilon(n) \nabla_{\rho_k(n)} \mathcal{L}, \quad (26)$$

$$\mathcal{L}(\boldsymbol{\rho}, \boldsymbol{\mu}, \boldsymbol{\nu}, \boldsymbol{\omega}) = \sum_{n=1}^N \sum_{k=1}^K BW_n \log_2 \left(1 + \frac{\rho_k |h_{n,k}|^2 \bar{p}_{n,k}}{\rho_k (|h_{n,k}|^2 \sum_{j \in \mathcal{K}, \bar{h}_{n,j} > \bar{h}_{n,k}} \bar{p}_{n,j} + |\sigma_{n,k}|^2) + C_{n,k}} \right) + \sum_{k=1}^K \mu_k \rho_k + \sum_{k=1}^K \nu_k (1 - \rho_k) + \sum_{k=1}^K \omega_k \left(\sum_{n=1}^N \eta (1 - \rho_k) \left(|h_{n,k}|^2 \sum_{j=1}^K \bar{p}_{n,j} + |\sigma_{n,k}|^2 \right) - E_{\text{req}} \right). \quad (21)$$

$$\nabla_{\rho_k} \mathcal{L} = \sum_{n=1}^N \frac{BW_n}{\ln 2} \cdot \frac{A_{n,k} C_{n,k}}{(A_{n,k} \rho_k + B_{n,k} \rho_k + C_{n,k})(B_{n,k} \rho_k + C_{n,k})} + \mu_k - \nu_k - \omega_k \sum_{n=1}^N \eta \left(|h_{n,k}|^2 \sum_{j=1}^K \bar{p}_{n,j} + |\sigma_{n,k}|^2 \right). \quad (25)$$

where $\rho_k(n)$ and $\rho_k(n+1)$ denote the ρ_k in the n -th and $(n+1)$ -th iteration respectively, and $\varepsilon(n)$ represents the updating step for ρ_k in the n -th iteration, which is required to satisfy the following condition

$$\varepsilon(n) = \arg \max_{\varepsilon} \mathcal{L}(\boldsymbol{\rho}(n+1), \boldsymbol{\mu}, \boldsymbol{\nu}, \boldsymbol{\omega}) \Big|_{\rho(n+1)=\rho(n)+\varepsilon \nabla_{\rho(n)} \mathcal{L}}. \quad (27)$$

Process in (26) is repeated until $|\nabla_{\rho_k(n)} \mathcal{L}| \leq \epsilon_1$ for any $k \in \mathcal{K}$, and the optimal PS ratio is denoted as $\boldsymbol{\rho}^*$. Therefore, the Lagrange dual objective function in (22) is further determined as

$$g(\boldsymbol{\mu}, \boldsymbol{\nu}, \boldsymbol{\omega}) = \mathcal{L}(\boldsymbol{\rho}^*, \boldsymbol{\mu}, \boldsymbol{\nu}, \boldsymbol{\omega}). \quad (28)$$

2) *Updating $\{\boldsymbol{\mu}, \boldsymbol{\nu}, \boldsymbol{\omega}\}$ With the Optimized $\boldsymbol{\rho}^*$* : With the obtained PS ratio $\boldsymbol{\rho}^*$, the corresponding optimal Lagrange multipliers $\{\boldsymbol{\mu}, \boldsymbol{\nu}, \boldsymbol{\omega}\}$ can be determined accordingly through solving the Lagrange dual problem in (23)-(24).

Obviously, the dual problem is convex on the set of Lagrange multipliers $\{\boldsymbol{\mu}, \boldsymbol{\nu}, \boldsymbol{\omega}\}$. Therefore, one-dimensional search scheme can be adopted to optimize the dual variables. Nevertheless, the objective function (23) is not necessarily differentiable and thus this gradient-based approach is not always feasible. Otherwise, we apply the widely-used sub-gradient method to determine the dual variables $\{\boldsymbol{\mu}, \boldsymbol{\nu}, \boldsymbol{\omega}\}$, for which the sub-gradient directions are given in *Proposition 2*.

Proposition 2: The sub-gradient of the Lagrange dual function regarding the Lagrange multipliers can be respectively calculated by

$$\nabla_{\mu_k} g = \rho_k^*, \quad (29)$$

$$\nabla_{\nu_k} g = 1 - \rho_k^*, \quad (30)$$

$$\nabla_{\omega_k} g = \sum_{n=1}^N \eta (1 - \rho_k^*) \left(|h_{n,k}|^2 \sum_{j=1}^K \bar{p}_{n,j} + |\sigma_{n,k}|^2 \right) - E_{\text{req}}. \quad (31)$$

Proof: Please refer to [32] for more details. ■

According to *Proposition 2*, the value of μ_k (ν_k , ω_k) should decrease if $\nabla_{\mu_k} g > 0$ ($\nabla_{\nu_k} g > 0$, $\nabla_{\omega_k} g > 0$), and vice versa. Based on this observation, we apply the binary search algorithm [32] with the error tolerance ϵ_2 to determine the optimal Lagrange multipliers (denoted as $\{\boldsymbol{\mu}^*, \boldsymbol{\nu}^*, \boldsymbol{\omega}^*\}$).

The algorithms developed in 1) and 2) operate alternately until the duality gap no longer changes, i.e.,

$$|R_{\text{sum}}(\boldsymbol{\rho}^*) - g(\boldsymbol{\mu}^*, \boldsymbol{\nu}^*, \boldsymbol{\omega}^*)| = \text{const}, \quad (32)$$

where *const* denotes a non-negative constant.

B. Power Allocation With Fixed PS Ratio

After obtaining the optimal solution of the PS ratio $\boldsymbol{\rho}^*$, now we aimed at optimizing the power allocation \mathbf{p} under the optimized $\boldsymbol{\rho}^*$. Correspondingly, the original optimization problem in (11)-(15) is predigested into the following sub-problem

$$\max_{\mathbf{p}} R_{\text{sum}}(\mathbf{p}) \quad (33)$$

$$\text{s.t.} \quad E_k \geq E_{\text{req}}, \quad \forall k \in \mathcal{K}, \quad (34)$$

$$p_{n,k} \geq 0, \quad \forall n \in \mathcal{N}, \quad \forall k \in \mathcal{K}, \quad (35)$$

$$\sum_{n=1}^N p_{n,k} \leq p_k^{\max}, \quad \forall k \in \mathcal{K}. \quad (36)$$

Proposition 3: Suppose that $|\sigma_{n,k}^{\text{ID}}|^2 \rightarrow 0$ and $|\sigma_{n,k}|^2 = |\sigma_{n,j}|^2 = |\sigma_n|^2 (\forall k, j \in \mathcal{K})$. The sub-problem (33)-(36) is convex if the feasible domain is non-empty.

Proof: Please refer to Appendix B. ■

Similar to section III.A, the Lagrangian duality based algorithm is also employed here to obtain the near-optimal power allocation \mathbf{p} .

Based on (67)-(69) given in Appendix B, the corresponding Lagrangian function for the sub-problem (33)-(36) can be written as (37) on the top of the next page, in which $\boldsymbol{\alpha} = [\alpha_1, \dots, \alpha_K]^T$, $\boldsymbol{\beta} = [\beta_1, \dots, \beta_N]^T$ with $\beta_n = [\beta_{n,1}, \dots, \beta_{n,K}]^T$ and $\boldsymbol{\gamma} = [\gamma_1, \dots, \gamma_K]^T$ are non-negative multipliers with respect to (34), (35) and (36), respectively.

Accordingly, the Lagrange dual objective function is given by

$$\tilde{g}(\boldsymbol{\alpha}, \boldsymbol{\beta}, \boldsymbol{\gamma}) = \max_{\mathbf{p}} \tilde{\mathcal{L}}(\mathbf{p}, \boldsymbol{\alpha}, \boldsymbol{\beta}, \boldsymbol{\gamma}), \quad (38)$$

Thus, the corresponding dual optimization problem can be formulated as follows

$$\min_{\boldsymbol{\alpha}, \boldsymbol{\beta}, \boldsymbol{\gamma}} \tilde{g}(\boldsymbol{\alpha}, \boldsymbol{\beta}, \boldsymbol{\gamma}) \quad (39)$$

$$\text{s.t.} \quad \boldsymbol{\alpha} \succeq \mathbf{0}, \boldsymbol{\beta} \succeq \mathbf{0}, \boldsymbol{\gamma} \succeq \mathbf{0}. \quad (40)$$

The proposed algorithm to solve the aforementioned problems consists of two steps, and more specific details are developed as follows.

1) *Optimizing \mathbf{p} Under Fixed Lagrange Multipliers $\{\boldsymbol{\alpha}, \boldsymbol{\beta}, \boldsymbol{\gamma}\}$* : The gradient ascent method is employed to de-

$$\begin{aligned} \tilde{\mathcal{L}}(\mathbf{p}, \boldsymbol{\alpha}, \boldsymbol{\beta}, \boldsymbol{\gamma}) &= \sum_{n=1}^N \sum_{i=1}^K BW_n \log_2 \left(1 + \frac{|h_{n,\pi(i)}|^2 p_{n,\pi(i)}}{|h_{n,\pi(i)}|^2 \sum_{j=i+1}^K p_{n,\pi(j)} + |\sigma_n|^2} \right) \\ &+ \sum_{i=1}^K \alpha_i \left(\sum_{n=1}^N \eta(1 - \rho_i^*) \left(|h_{n,\pi(i)}|^2 \sum_{j=1}^K p_{n,\pi(j)} + |\sigma_n|^2 \right) - E_{\text{req}} \right) + \sum_{n=1}^N \sum_{i=1}^K \beta_{n,i} p_{n,\pi(i)} + \sum_{i=1}^K \gamma_i \left(p_k^{\max} - \sum_{n=1}^N p_{n,\pi(i)} \right). \end{aligned} \quad (37)$$

$$\begin{aligned} \nabla_{p_{n,\pi(i)}} \tilde{\mathcal{L}} &= \frac{BW_n}{\ln 2} \cdot \left(\frac{|h_{n,\pi(1)}|^2}{|h_{n,\pi(1)}|^2 \Theta_{n,\pi(1)} + |\sigma_n|^2} + \sum_{i'=2}^i \left(\frac{|h_{n,\pi(i')}|^2}{|h_{n,\pi(i')}|^2 \Theta_{n,\pi(i')} + |\sigma_n|^2} - \frac{|h_{n,\pi(i'-1)}|^2}{|h_{n,\pi(i'-1)}|^2 \Theta_{n,\pi(i')} + |\sigma_n|^2} \right) \right) \\ &+ \beta_{n,i} - \gamma_i + \sum_{j=1}^K \alpha_j \eta(1 - \rho_j^*) |h_{n,\pi(j)}|^2. \end{aligned} \quad (41)$$

termine the optimal power allocation \mathbf{p}^* . Firstly, we analyze the gradient direction of the Lagrangian function given in (37) with regard to the power allocation component $p_{n,\pi(i)}$, which is calculated as (41) on the top of the next page.

On the n -th ($1 \leq n \leq N$) subchannel, the power allocation for each MU can be successively updated through the following expressions

$$\begin{aligned} \underbrace{p_{n,\pi(1)}(1) \rightarrow p_{n,\pi(K)}(1)}_{\text{The 1-st iteration}} \rightarrow \underbrace{p_{n,\pi(1)}(t) \rightarrow p_{n,\pi(K)}(t)}_{\text{The } t\text{-th iteration}} \\ \rightarrow \underbrace{p_{n,\pi(1)}(t+1) \rightarrow p_{n,\pi(K)}(t+1)}_{\text{The } (t+1)\text{-th iteration}}, \end{aligned} \quad (42)$$

$$p_{n,\pi(i)}(t+1) = p_{n,\pi(i)}(t) + \tilde{\varepsilon}(t) \nabla_{p_{n,\pi(i)}(t)} \tilde{\mathcal{L}}, \quad (43)$$

where t and $t+1$ indicate the number of iterations; and $\tilde{\varepsilon}(t)$ represents the updating step in the t -th iteration, which is obtained through a similar way to $\varepsilon(t)$ (given by equation (27)).

The updating process (42)-(43) for the power allocation on the n -th subchannel proceeds until $|\nabla_{p_{n,\pi(i)}} \tilde{\mathcal{L}}| \leq \epsilon_3$ for any $1 \leq i \leq K$. Correspondingly, the optimal power allocation on the n -th subcarrier is expressed as \mathbf{p}_n^* and thus $\mathbf{p}^* = [\mathbf{p}_1^*, \dots, \mathbf{p}_N^*]^T$. Then, the dual objective function in (38) can be reformulated as

$$\tilde{g}(\boldsymbol{\alpha}, \boldsymbol{\beta}, \boldsymbol{\gamma}) = \tilde{\mathcal{L}}(\mathbf{p}^*, \boldsymbol{\alpha}, \boldsymbol{\beta}, \boldsymbol{\gamma}). \quad (44)$$

2) *Optimizing $\{\boldsymbol{\alpha}, \boldsymbol{\beta}, \boldsymbol{\gamma}\}$ Under the Obtained \mathbf{p}^** : Similar to section III.A, sub-gradient approach is employed here to tackle the optimization of Lagrange multipliers $\{\boldsymbol{\alpha}, \boldsymbol{\beta}, \boldsymbol{\gamma}\}$, for which the sub-gradient directions are respectively denoted as follows

$$\nabla_{\alpha_i} \tilde{g} = \sum_{n=1}^N \eta(1 - \rho_i^*) \left(|h_{n,\pi(i)}|^2 \sum_{j=1}^K p_{n,\pi(j)} + |\sigma_n|^2 \right) - E_{\text{req}}, \quad (45)$$

$$\nabla_{\beta_{n,i}} \tilde{g} = p_{n,\pi(i)}, \quad (46)$$

$$\nabla_{\gamma_i} \tilde{g} = p_k^{\max} - \sum_{n=1}^N p_{n,\pi(i)}. \quad (47)$$

The binary search method with the error tolerance ϵ_4 is applied to determine the optimal solution of the Lagrange multipliers here, which are denoted as $\{\boldsymbol{\alpha}^*, \boldsymbol{\beta}^*, \boldsymbol{\gamma}^*\}$.

The algorithms developed in 1) and 2) are repeated alternately until the duality gap no longer changes, i.e.,

$$|R_{\text{sum}}(\mathbf{p}^*) - \tilde{g}(\boldsymbol{\alpha}^*, \boldsymbol{\beta}^*, \boldsymbol{\gamma}^*)| = \text{const}. \quad (48)$$

C. Complete Solution for Joint Power Allocation and Splitting Control

Up to now, the solutions to the sub-problems for optimizing $\boldsymbol{\rho}$ and \mathbf{p} have been proposed in section III.A and III.B, respectively. Now we develop the complete solution for jointly optimizing the original problem (11)-(15), which is summarized in Algorithm 1.

Proposition 4: The complete solution converges to an optimal set of $\{\boldsymbol{\rho}^*, \mathbf{p}^*\}$ which maximizes the achievable data rate of the system to $R_{\text{sum}}(\boldsymbol{\rho}^*, \mathbf{p}^*)$.

Proof: Suppose that the solution (not the optimal solution of problem (11)-(15)) in the l -th iteration of Algorithm 1 is denoted as $\{\boldsymbol{\rho}^{(l)}, \mathbf{p}^{(l)}\}$ and the corresponding achievable data rate of the system is $R_{\text{sum}}(\boldsymbol{\rho}^{(l)}, \mathbf{p}^{(l)})$. The process in the $(l+1)$ -th iteration is described as follows:

1) Under the fixed power allocation $\mathbf{p}^{(l)}$, we optimize the PS ratio assignment and denote it as $\boldsymbol{\rho}^{(l+1)}$. Hence, the corresponding achievable data rate of the system is written as $R_{\text{sum}}(\boldsymbol{\rho}^{(l+1)}, \mathbf{p}^{(l)})$. It is necessary that $R_{\text{sum}}(\boldsymbol{\rho}^{(l+1)}, \mathbf{p}^{(l)}) \geq R_{\text{sum}}(\boldsymbol{\rho}^{(l)}, \mathbf{p}^{(l)})$ always holds, otherwise $\boldsymbol{\rho}^{(l+1)}$ is not the optimal solution to the sub-problem (16)-(18) in the $(l+1)$ -th iteration. This is because that there exists at least one other solution, such as $\boldsymbol{\rho}^{(l)}$, which enables the objective function to achieve a larger value, i.e., $R_{\text{sum}}(\boldsymbol{\rho}^{(l+1)}, \mathbf{p}^{(l)}) < R_{\text{sum}}(\boldsymbol{\rho}^{(l)}, \mathbf{p}^{(l)})$.

2) Under the fixed PS ratio $\boldsymbol{\rho}^{(l+1)}$, we then optimize the power allocation which is indicated as $\mathbf{p}^{(l+1)}$. Accordingly, the achievable data rate of the system is written as $R_{\text{sum}}(\boldsymbol{\rho}^{(l+1)}, \mathbf{p}^{(l+1)})$. It is necessary that the expression $R_{\text{sum}}(\boldsymbol{\rho}^{(l+1)}, \mathbf{p}^{(l+1)}) \geq R_{\text{sum}}(\boldsymbol{\rho}^{(l+1)}, \mathbf{p}^{(l)})$ always holds. The

Algorithm 1 Complete Solution for Joint Power Allocation and Splitting Control

- 1: Initialize $\bar{\mathbf{p}}$ and stop criteria $\epsilon_1, \epsilon_2, \epsilon_3, \epsilon_4$.
 - 2: **repeat**
 - 3: *Step 1: optimize the PS ratio under fixed power allocation:*
 - 4: **repeat**
 - 5: initialize dual variables $\{\boldsymbol{\mu}, \boldsymbol{\nu}, \boldsymbol{\omega}\}$;
 - 6: solve the problem (22) to obtain the optimal $\boldsymbol{\rho}^*$ according to (25)-(26) until $|\nabla_{\rho_k(n)} \mathcal{L}| \leq \epsilon_1 (\forall k \in \mathcal{K})$;
 - 7: determine the optimal dual variables $\{\boldsymbol{\mu}^*, \boldsymbol{\nu}^*, \boldsymbol{\omega}^*\}$ according to *Proposition 2*;
 - 8: **until** $R_{\text{sum}}(\boldsymbol{\rho}^*) = g(\boldsymbol{\mu}^*, \boldsymbol{\nu}^*, \boldsymbol{\omega}^*)$.
 - 9: *Step 2: optimize the power allocation with fixed PS ratio:*
 - 10: **repeat**
 - 11: initialize the PS ratio assignment as $\boldsymbol{\rho}^*$;
 - 12: solve the problem (38) to acquire the optimal power allocation \mathbf{p}^* according to (41)-(43) until $|\nabla_{p_n, \pi(i)} \tilde{\mathcal{L}}| \leq \epsilon_3 (\forall i \in \mathcal{K})$;
 - 13: determine the optimal dual variables $\{\boldsymbol{\alpha}^*, \boldsymbol{\beta}^*, \boldsymbol{\gamma}^*\}$ according to (45)-(47);
 - 14: **until** $R_{\text{sum}}(\mathbf{p}^*) = \tilde{g}(\boldsymbol{\alpha}^*, \boldsymbol{\beta}^*, \boldsymbol{\gamma}^*)$.
 - 15: **until** $R_{\text{sum}}(\boldsymbol{\rho}^*) = R_{\text{sum}}(\mathbf{p}^*)$.
-

reason for this is similar to that described in 1), and hence it is omitted here for the sake of simplicity.

In short, it can be concluded that

$$R_{\text{sum}}(\boldsymbol{\rho}^{(l+1)}, \mathbf{p}^{(l+1)}) \geq R_{\text{sum}}(\boldsymbol{\rho}^{(l)}, \mathbf{p}^{(l)}) \geq \dots \geq R_{\text{sum}}(\boldsymbol{\rho}^{(1)}, \mathbf{p}^{(1)}). \quad (49)$$

On the other hand, it is impossible that the achievable data rate of the considered system grows infinitely owing to the transmit power limitation. Hence, as the number of the iterations increases, we have

$$R_{\text{sum}}(\boldsymbol{\rho}^{(l+1)}, \mathbf{p}^{(l+1)}) \rightarrow R_{\text{sum}}(\boldsymbol{\rho}^*, \mathbf{p}^*), \quad (50)$$

which completes the proof of *Proposition 4*. \blacksquare

The complete algorithm can be regarded as a dual-layer process. In the inner-layer, the complexity of the gradient decent algorithm is $\mathcal{O}(K)$ and the number of this loop iteration is approximately $\mathcal{O} \log(1/\epsilon_1^2)$ [33]; and the complexity of the binary search method with error tolerance ϵ_2 is $\mathcal{O} \log(1/\epsilon_2^2)$. Similarly, in the outer-layer, the computational complexity of the gradient algorithm method is $\mathcal{O}(NK)$ and the number of this loop iteration is approximately $\mathcal{O} \log(1/\epsilon_3^2)$; and the complexity of the binary search method is $\mathcal{O} \log(1/\epsilon_4^2)$. To summarize, the computational complexity of the complete solution is $\mathcal{O}(NK^2 \log(1/\epsilon_1^2) \log(1/\epsilon_2^2) \log(1/\epsilon_3^2) \log(1/\epsilon_4^2))$.

IV. ALTERNATIVE ALGORITHM BASED ON DEEP LEARNING

Since the computational complexity of the complete algorithm summarized in Algorithm 1 grows considerably as the number of MUs and subchannels increases, it is difficult to simultaneously satisfy the demands for high data rate and low latency. To get over this difficulty, we propose an alternative

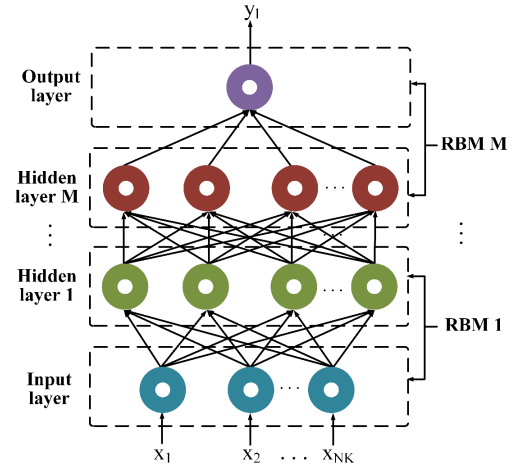


Fig. 2: An example of the framework of DBN.

approach based on empirical data and the deep learning framework to obtain the approximate solution that maximizes the achievable data rate of the considered SWIPT-aided MC-NOMA system. In particular, we choose DBN to complete the deep learning-based approach due to its capability of modelling highly abstracted dependencies between the inputs and the outputs. In the conventional deep neural networks (DNNs), as the depth of the network increases, it is easy to fall into a local minimum while iterating, and thus causing the failure of training. Compared to the conventional DNNs, DBN is a multi-layer neural network composed of several RBMs, which are pre-trained one by one before stacking into a DBN. The major advantage is that before supervised training with back-propagation algorithm, the network parameters can be initialized to a better local optimal point or even the global optimal point through the process of unsupervised pre-training. Therefore, we apply the DBN to complete the deep learning-based approach.

First of all, we make a brief introduction to the DBN, which is one of the typical deep learning models and can effectively capture the intrinsic relationship between the input and the output data [34]. As presented in Fig. 2, the model of DBN contains an input layer, several hidden layers and an output layer, among which two adjacent layers (serving as visible layer and hidden layer respectively) are regarded as a restricted Boltzmann machine (RBM). Note that the neurons between two adjacent layers are fully connected while the neurons in the same layer are disconnected from each other.

Then, we develop the DBN-based learning algorithm including preparation, training and running, which are presented as follows.

1) *Data preparation phase – to obtain the training set and the testing set.* Since the DBN-based learning method is based on a considerably great amount of empirical data, we first prepare a data set in this part, which includes the input and the corresponding output of the DBN model. In this work, the vector of the randomly generated channel gains serves as

the input \mathbf{x} of the DBN. Besides, the output y_l of the DBN is provided by the corresponding optimal solution $\{\mathbf{p}^*, \boldsymbol{\rho}^*\}$, which is obtained through the complete algorithm developed in Section III or the well-known genetic algorithm.

Note that the BS communicates with K MUs through N subchannels in our considered MC-NOMA network, the set of optimal solution $\{\boldsymbol{\rho}^*, \mathbf{p}^*\}$ is composed of $NK + K$ components. Hence, it is required to estimate totally $NK + K$ parameters through the well-trained DBNs, which are denoted as DBN_l ($1 \leq l \leq NK + K$).

2) *Training phase – to establish a well-trained DBN for each component of $\{\boldsymbol{\rho}^*, \mathbf{p}^*\}$.* After obtaining lots of data samples in the previous part, now we turn to train DBN_l one by one. The process of the training involves two stage, i.e., *unsupervised learning and supervised learning*. Let \mathbf{v} and \mathbf{h} respectively represent the visible and the hidden layer of the RBM in DBN_l . Denote $\Psi = \{\mathbf{w}, \mathbf{b}_v, \mathbf{b}_h\}$, in which \mathbf{w} denotes the weight between \mathbf{v} and \mathbf{h} while \mathbf{b}_v and \mathbf{b}_h respectively denote the biases related to the \mathbf{v} and \mathbf{h} .

In the unsupervised learning phase, the set Ψ is updated according to the following formula

$$\Psi^{(t+1)} = \Psi^{(t)} + \xi \frac{\partial \log \Pr(\mathbf{v}^{(t)})}{\partial \Psi^{(t)}}, \quad (51)$$

in which t and ξ indicate the number of updates and the corresponding learning rate, respectively. Besides, $\Pr(\mathbf{v}^{(t)})$ represents the probability distribution of $\mathbf{v}^{(t)}$ and can be determined according to the joint probability distribution $\Pr(\mathbf{v}^{(t)}, \mathbf{h}^{(t)})$, which is given by

$$\begin{aligned} \Pr(\mathbf{v}^{(t)}) &= \sum_{\mathbf{h}^{(t)}} \Pr(\mathbf{v}^{(t)}, \mathbf{h}^{(t)}) \\ &= \sum_{\mathbf{h}^{(t)}} \frac{\exp(-E(\mathbf{v}^{(t)}, \mathbf{h}^{(t)}))}{\sum_{\mathbf{v}^{(t)}} \sum_{\mathbf{h}^{(t)}} \exp(-E(\mathbf{v}^{(t)}, \mathbf{h}^{(t)}))}. \end{aligned} \quad (52)$$

In (52), $E(\mathbf{v}^{(t)}, \mathbf{h}^{(t)})$ denotes the energy function of $\mathbf{v}^{(t)}$ and $\mathbf{h}^{(t)}$, which is calculated by

$$E(\mathbf{v}^{(t)}, \mathbf{h}^{(t)}) = -\mathbf{v}'^{(t)} \mathbf{w}^{(t)} \mathbf{h}^{(t)} - \mathbf{b}_v'^{(t)} \mathbf{v}^{(t)} - \mathbf{b}_h'^{(t)} \mathbf{h}^{(t)}. \quad (53)$$

In the supervised learning phase, the set Ψ is fine-tuned based on the back-propagation method, which is written by

$$\Psi^{(t'+1)} = \Psi^{(t')} - \tilde{\xi} \frac{\partial \mathcal{S}_l}{\partial \Psi^{(t')}}, \quad (54)$$

in which t' and $\tilde{\xi}$ indicate the number of fine-tunings and the corresponding learning rate. Besides, \mathcal{S}_l represents the cross entropy which is applied to measure the estimation error of DBN_l . Mathematically, the fine-tuning procedure is equivalent to the cross entropy minimization problem, and the cross entropy \mathcal{S}_l is given by

$$\mathcal{S}_l = -\frac{1}{D} \sum_{i=1}^D \left(y_l^{(i)} \log(\hat{y}_l^{(i)}) + (1 - y_l^{(i)}) \log(1 - \hat{y}_l^{(i)}) \right), \quad (55)$$

in which D is the size of the data set used to train DBN_l . Besides, $y_l^{(i)}$ is the output of the i -th data sample and $\hat{y}_l^{(i)}$ denotes the output that estimated by DBN_l with the input $\mathbf{x}^{(i)}$.

3) *Running phase – to obtain the approximated solution based on the well-trained DBNs.* In this part, the DBNs that have been fully trained are loaded to estimate the solution to the optimization problem (11)-(15). First of all, the channel coefficients $h_{n,k}$ ($n \in \mathcal{N}$, $k \in \mathcal{K}$) are randomly generated and the input layers of all DBNs are given by $\mathbf{x} = [h_{1,1}, \dots, h_{1,K}, \dots, h_{N,1}, \dots, h_{N,K}]^T$. With the fully-trained DBN_l ($1 \leq l \leq NK + K$) and the input \mathbf{x} , the output of DBN_l can be calculated directly, which is denoted as \hat{y}_l ($1 \leq l \leq NK + K$). Thus, the approximated solution to the original problem (11)-(15) is formed as follows

$$\hat{\boldsymbol{\rho}} = [\hat{y}_1, \dots, \hat{y}_K]^T, \quad (56)$$

$$\hat{\mathbf{p}} = [\hat{y}_{K+1}, \dots, \hat{y}_{2K}, \dots, \hat{y}_{NK+1}, \dots, \hat{y}_{NK+K}]^T. \quad (57)$$

To summarize, the alternative DBN-based learning approach is presented in Algorithm 2.

Algorithm 2 Learning Approach to Approximating the Power Allocation and Splitting Control

- 1: Initialize the stop criteria ϵ_5 and ϵ_6 .
 - 2: **Data preparation part:**
 - 3: generate plenty of training data samples $\{\mathbf{x}, \mathbf{y}\}$.
 - 4: **Network training part:**
 - 5: **for** $l = 1 : NK + K$
 - 6: **for** $m = 1 : M$
 - 7: initialize the parameter set Ψ for the m -th RBM;
 - 8: *i. unsupervised learning phase:*
 - 9: **repeat**
 - 10: calculate Ψ according to (51);
 - 11: **until** $\|\Psi^{(t+1)} - \Psi^{(t)}\| \leq \epsilon_5$;
 - 12: *ii. supervised learning phase:*
 - 13: **repeat**
 - 14: fine-tune Ψ according (54);
 - 15: **until** $\|\Psi^{(t'+1)} - \Psi^{(t')}\| \leq \epsilon_6$.
 - 16: **end**
 - 17: **end**
 - 18: **Solution running part:**
 - 19: generate channel gains randomly and denote $\mathbf{x} = [h_{1,1}, \dots, h_{1,K}, \dots, h_{N,1}, \dots, h_{N,K}]^T$;
 - 20: load the well-trained DBNs;
 - 21: **for** $l = 1 : NK + K$
 - 22: estimate \hat{y}_l according to the input \mathbf{x} and the well-trained DBN_l ;
 - 23: **end**
 - 24: form the approximation of solution $\hat{\boldsymbol{\rho}}$ and $\hat{\mathbf{p}}$ according to (56)-(57).
-

V. NUMERICAL RESULTS

In this section, simulation results are provided to examine the superiority of the considered downlink SWIPT-aided MC-NOMA system in terms of achievable data rate of the system,

where the effectiveness of our developed iterative algorithm and deep learning-based is evaluated. Suppose that the BS is placed in the center of a circular cell with a radius of 300m and all MUs are randomly and independently distributed within the cell. The total frequency band of the system is set to $BW = 100\text{MHz}$. Referring to the classic 3GPP propagation environment [35], the transmission channel between a pair of transceivers consists of i.i.d Rayleigh block fading, Log-Normal shadowing with standard deviation of 8 dB and path loss given by $(\frac{d_0}{d})^v$. In particular, d represents the actual propagation distance from the BS to the MU, $d_0 = 2.5$ corresponds to the reference distance and $v = 3.76$ represents the path-loss exponent, respectively. Besides, the power spectrum density (PSD) of the channel noise is assumed to -96dBm/Hz and the PSD of the additional noise emerged during power splitting is assumed to -192dBm/Hz . The loss of the EH receivers is set to $\eta = 38\%$.

The widely-known programming tool *Tensorflow r1.8* is adopted, which is implemented in the platform *Python 3.6.0* to perform the constructing, training and running of the DBN models. Specifically, 10000 data samples $\{\mathbf{x}, \mathbf{y}\}$ are prepared to train the DBNs in each case of various system parameters setting. The number of neurons of each hidden layer in the DBN model is taken as 32, 64 and 32, respectively. Additionally, the learning rates in the unsupervised training and the supervised training are taken as $\xi = 1e^{-4}$ and $\xi = 1e^{-4}$ respectively; the number of training epoches is taken as 3000; and the precisions in the unsupervised training and the supervised training are set to $\epsilon_5 = 1e^{-3}$ and $\epsilon_6 = 1e^{-3}$, respectively.

In the first simulation, we investigate the convergence performance of the developed Lagrangian duality-based approach, and measure the effectiveness of the proposed DBN-based learning algorithm. We take a SWIPT-based MC-NOMA system with two subchannels and two MUs as an example, where the maximum power supply of the BS and the minimum demand for EH are set to 4W and 0.01J respectively. As shown in Fig. 3, it is evident that the proposed Lagrangian duality-based approach is gradually converged to the optimal value acquired by the exhaustive search algorithm. This confirms our theoretical analysis of the convergence performance of our developed approach. On the other hand, the achievable data rate obtained by the proposed DBN-based learning approach is very close to the optimal value, approximately with the gap of 0.08. Although there is a certain gap between the DBN-based approximation and the optimal solution, it is acceptable to some extent because the sacrifice of a small amount of achievable data rate can bring a great improvement in processing efficiency, which is beneficial for the systems with strict requirement for low latency.

Then, we examine the performance of the proposed Lagrangian duality-based approach as well as DBN-based learning approach with different number of MUs. In this simulation, the available transmit power supply and the EH constraint for each MU are set to 10W and 0.01J, respectively. As shown in Fig. 4, the maximum achievable data rate of the system achieved by our developed schemes is monotonically non-

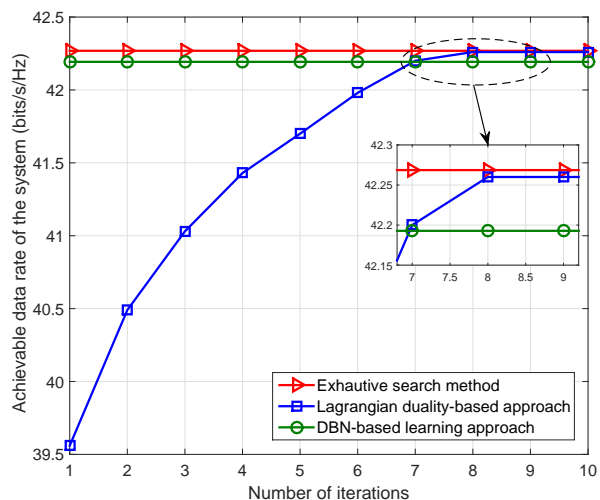


Fig. 3: The convergence behavior of the proposed Lagrangian duality-based approach and the effectiveness evaluation of the proposed DBN-based learning approach.

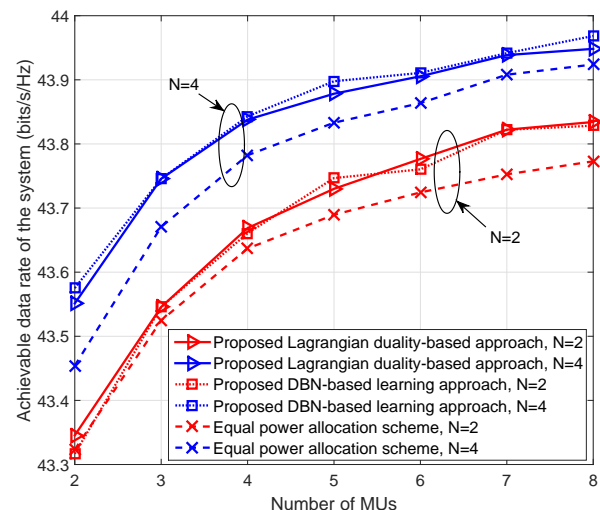


Fig. 4: Performance evaluation of the proposed Lagrangian duality-based and DBN-based approaches (achievable data rate of the system vs number of MUs).

decreasing as the number of MUs grows. More specifically, the achievable data rate of the system grows dramatically with a small number of MUs, and then slowly approaches an asymptote. This is because that the co-channel interference, which can be fully utilized by the EH receivers, enhances as the number of MUs grows. Hence, a smaller value of PS ratio for EH is needed to fulfill the demand for EH. Accordingly, the PS ratio for ID becomes larger, leading to the increase in the data rate. However, in the power-limited system, the achievable data rate of the system is bounded and hence it tends to converge to an asymptote at last. Besides, the results achieved by the DBN-based learning approach are very close to those achieved by the Lagrangian duality-based method.

In the next simulation, the performance of the developed schemes with diverse constraints is evaluated. Two different

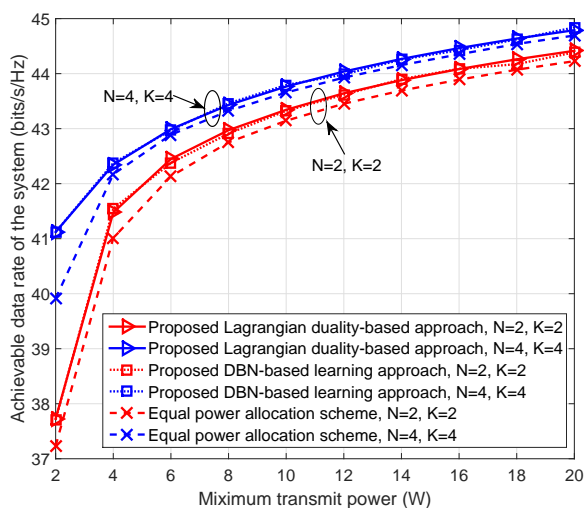


Fig. 5: Performance evaluation of the proposed Lagrangian duality-based and DBN-based approaches (achievable data rate of the system vs maximum transmit power).

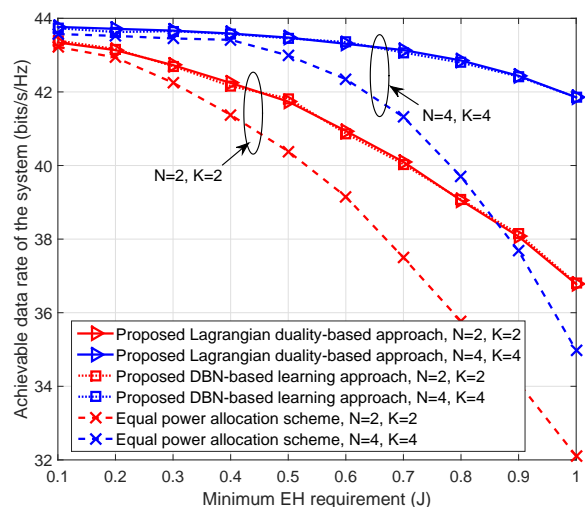


Fig. 6: Performance evaluation of the proposed Lagrangian duality-based and DBN-based approaches (achievable data rate of the system vs minimum EH requirement).

scenario settings are taken for comparison, i.e., $N = 2, K = 2$ and $N = 4, K = 4$. We firstly focus on the influence of the power budget on the achievable data rate of the system. Suppose that the EH constraint for each MU is $E_{\text{req}} = 0.1\text{J}$ and the transmit power budget varies from 2W to 20W. It is clearly presented in Fig. 5 that the maximum achievable data rate of the system is monotonically increasing with the growth of the transmit power supply. The reason is that as the available transmit power increases, the received signal is more likely to be used for ID once the EH demand for each MU is fulfilled, leading to the improvement in the achievable data rate of each MU and the system. Then we investigate the performance under different minimum EH requirements. Specifically, it is assumed that the available power supply is limited to 10W and the EH requirement changes from 0.1J to 1J. It is depicted in Fig. 6 that the achievable data rate of the system declines with increasing minimum EH requirement. This results from the fact that the received signal is more likely to be collected by the EH receivers to meet the demand for EH and accordingly the signal for ID is cut off. Similarly, the results derived from the DBN-based learning approach are also in line with the near-optimal results obtained by the Lagrangian duality-based method, which further demonstrates the validity of the DBN-based learning approach. Furthermore, we can conclude from Fig. 4-6 that our proposed approaches are superior to the equal power allocation scheme in terms of achievable data rate of the system.

Finally, the performance comparison in terms of maximum achievable data rate of the system is investigated among our proposed PS-based MC-NOMA and other schemes in the existing literatures. Specifically, the proposed scheme is compared to 1) the PS-based OMA scheme [36] to demonstrate the improvement of NOMA over OMA; 2) PS-based SC-NOMA scheme [37] to illustrate the superiority of MC-NOMA over SC-NOMA; and 3) the TS-based MC-NOMA [38] to evaluate the suitability of different types of SWIPT scheme. Fig. 7

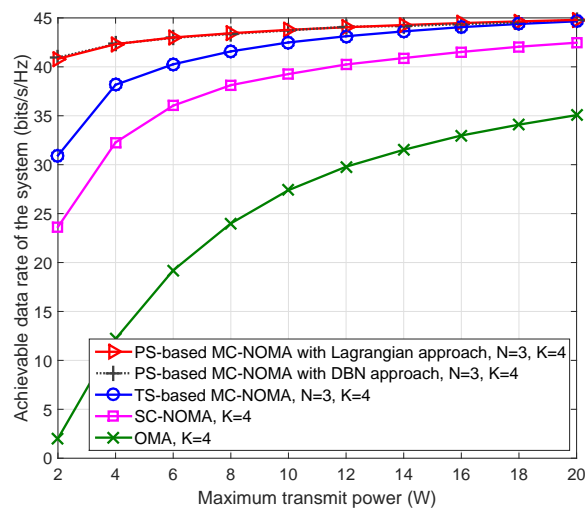


Fig. 7: Performance comparison in terms of achievable data rate of the system among different system model - OMA, SC-NOMA, TS-based MC-NOMA and PS-based MC-NOMA, $K=4$

shows the performance comparison under various available power budget. The demand for EH of each MU and the number of MUs are set to $E_{\text{req}} = 0.1\text{J}$ and $K = 4$ respectively, and the number of subchannels for two MC-NOMA systems is set to $N = 3$. It can be clearly seen in Fig. 7 that the PS-based NOMA schemes, including SC-NOMA and MC-NOMA, always outperform the PS-based OMA scheme in terms of achievable data rate of the system, which indicates that the NOMA system is more spectrum-efficient than the OMA system. More importantly, the PS-based MC-NOMA system is superior to the PS-based SC-NOMA system, which demonstrates the advantage of multi-carrier waveform for enhancing the performance of the achievable data rate of the system. In Fig. 8, we consider the simulation with a

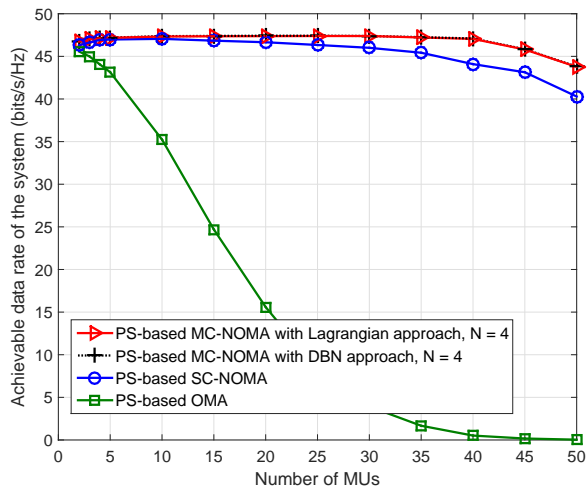


Fig. 8: Performance comparison among PS-based MC-NOMA, SC-NOMA and OMA under various number of MUs (achievable data rate of the system *vs* number of MUs).

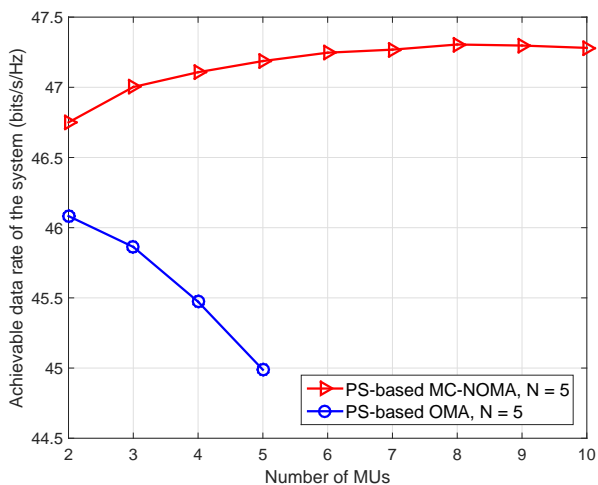


Fig. 9: Performance comparison for the case where the number of MUs in MC-NOMA is larger than that in OMA.

larger number of MUs, which is more in line with the actual communication application scenarios such as IoT and mMTC. Specifically, the performance comparison among MC-NOMA, SC-NOMA and OMA with PS-based SWIPT under different number of MUs is conducted, in which the demand for EH of each MU is set to $E_{\text{req}} = 0.1\text{J}$ and the number of subchannels for MC-NOMA scheme is set to $N = 4$. It can be observed from Fig. 8 that for the considered PS-based MC-NOMA scheme, the achievable data rate of the system first increases as the number of MUs increases, and then it gradually decreases as the number of MUs continues to increase. The reason for the decrease in the achievable data rate is that when the number of MUs exceeds a certain range, the total EH demand for the whole system is too large that it cannot be satisfied by intra-interference alone. Thus, extra power is required to achieve the EH requirement, which decreases the achievable data rate. More importantly, Fig. 8 shows that the

proposed PS-based MC-NOMA scheme outperforms both the PS-based SC-NOMA and the PS-based OMA in terms of achievable data rate of the system, and hence the advantage of SWIPT enabled MC-NOMA has been demonstrated. In Fig. 9, with a fixed number of subchannels (i.e., $N = 5$), the performance comparison between PS-based MC-NOMA and PS-based OMA is conducted. Note that in OMA scheme, the maximum number of MUs is 5 if $N = 5$, otherwise the orthogonality of the channel cannot be guaranteed. As shown in Fig. 9, it is clear that the proposed MC-NOMA scheme always outperforms OMA scheme regardless of the number of users, which demonstrates the superiority of MC-NOMA to OMA in terms of both the performance of achievable data rate and the number of serving users.

VI. CONCLUSIONS

In this paper, we have investigated the achievable data rate maximization problem for the downlink SWIPT-aided MC-NOMA system with PS receivers under the constraints of the maximum transmit power budget and the minimum EH requirement. The coupling of multiple variables as well as the presence of co-channel interference resulted in the fact that the maximization problem was non-convex and therefore it was strenuous to obtain the optimal solution directly. To tackle this problem, we proposed a decoupled approach where the coupled variables, i.e., the power allocation and the PS ratio assignment, were separated. Then the corresponding sub-problems were solved by employing the Lagrangian duality-based method. An alternative approach based on deep learning technique was then put forward to obtain the approximated solution to the original problem. Numerical results demonstrated that the proposed approaches outperformed the equal power allocation scheme. More importantly, it was confirmed that the considered PS-based MC-NOMA was superior to other existing schemes in terms of the performance of the achievable data rate of the system, including PS-based SC-NOMA and PS-based OMA.

Nevertheless, the complexity of SIC in MC-NOMA system is significantly higher than that in SC-NOMA, especially for large number of users in practical 5G communication application scenarios, which is the main challenge in using MC-NOMA over SC-NOMA with SWIPT. Therefore, our future concern includes implementing a promising solution with considerably lower complexity in a dense scenario. Furthermore, owing to the fact the EE optimization balances the achievable data rate and the power consumption of the system and accordingly it is consistent with the concept of green communication, the EE optimization problem for a non-linear power model will also be considered in the future work, where subchannel scheduling, power allocation and splitting will be jointly considered.

APPENDIX A

PROOF OF PROPOSITION 1

To certify the convexity of the optimization (16)-(18), we first check that the feasible PS ratio region is non-empty and convex. The feasible region of PS ratio is non-empty due to the

restriction in (20), and its convexity can be acquired according to (18) and (19).

Then we come to prove that the objective function in (16) is concave on ρ . Let

$$A_{n,k} = |h_{n,k}|^2 \bar{p}_{n,k}, \quad (58)$$

$$B_{n,k} = |h_{n,k}|^2 \sum_{\substack{j \in \mathcal{K}, \\ \tilde{h}_{n,j} > h_{n,k}}} \bar{p}_{n,j} + |\sigma_{n,k}|^2, \quad (59)$$

$$C_{n,k} = |\sigma_{n,k}^{\text{ID}}|^2. \quad (60)$$

Thus, (16) is further simplified as follow

$$\begin{aligned} R_{\text{sum}}(\rho) &= \sum_{n=1}^N R_n \\ &= \sum_{n=1}^N \sum_{k=1}^K BW_n \log_2 \left(1 + \frac{A_{n,k} \rho_k}{B_{n,k} \rho_k + C_{n,k}} \right), \end{aligned} \quad (61)$$

where $R_n = \sum_{k=1}^K BW_n \log_2 \left(1 + \frac{A_{n,k} \rho_k}{B_{n,k} \rho_k + C_{n,k}} \right)$ denotes the achievable data rate on the n -th subchannel.

Then the first-order derivative of R_n with respect to ρ_k is calculated by

$$\frac{\partial R_n}{\partial \rho_k} = \frac{BW_n}{\ln 2} \cdot \frac{A_{n,k} C_{n,k}}{(A_{n,k} \rho_k + B_{n,k} \rho_k + C_{n,k})(B_{n,k} \rho_k + C_{n,k})}. \quad (62)$$

Furthermore, the second-order derivative of R_n with respect to ρ_k is given by (63)-(64) on the top of the next page. Let $H_k = \frac{\partial^2 R_n}{\partial \rho_k^2}$. Hence, the corresponding Hessian matrix \mathbf{H} is given by

$$\mathbf{H} = \begin{bmatrix} H_1 & 0 & \cdots & 0 \\ 0 & H_2 & \cdots & 0 \\ \vdots & \vdots & \ddots & \vdots \\ 0 & 0 & 0 & H_K \end{bmatrix}. \quad (65)$$

Denote $\mathbf{Q} = -\mathbf{H}$ and the m -th order principal minor of the matrix \mathbf{Q} can be denoted as follow

$$Q_m = \begin{vmatrix} -H_1 & 0 & 0 & 0 \\ 0 & -H_2 & 0 & 0 \\ \vdots & \vdots & \ddots & \vdots \\ 0 & 0 & \cdots & -H_m \end{vmatrix} = (-1)^m \prod_{j=1}^m H_j. \quad (66)$$

According to (63), it is clear that $H_k \leq 0$ for all $k \in \mathcal{K}$. Hence, $Q_m \geq 0$ ($1 \leq m \leq K$) always holds, which indicates that $\mathbf{Q} = -\mathbf{H} \succeq \mathbf{0}$ and correspondingly $\mathbf{H} \preceq \mathbf{0}$. Consequently, it can be concluded that R_n is concave with regard to ρ .

Since the finite summation of concave functions will maintain the concavity, the objective function $R_{\text{sum}}(\rho)$ in (16) is concave on ρ . This completes the proof of Proposition 1. ■

APPENDIX B

PROOF OF PROPOSITION 3

Note that the feasible domain of the sub-problem (33)-(36) is assumed to be non-empty and its convexity can be clearly derived according to the constraints in (34)-(36).

Then we turn to analyze the concavity of the objective function (33) with regard to \mathbf{p} . Specifically, we define the relationship between the k -th MU and its decoding order as $k = \pi(i)$. Since $|\sigma_{n,k}^{\text{ID}}|^2$ is negligibly small and $|\sigma_{n,k}|^2 = |\sigma_{n,j}|^2 = |\sigma_n|^2$ ($\forall k, j \in \mathcal{K}$), the objective function can be further reduced as

$$R_{\text{sum}}(\mathbf{p}) = \sum_{n=1}^N R_n, \quad (67)$$

where

$$\begin{aligned} R_n &= \sum_{k=1}^K BW_n \log_2 \left(1 + \frac{|h_{n,k}|^2 p_{n,k}}{|h_{n,k}|^2 \sum_{\substack{j \in \mathcal{K}, \\ \tilde{h}_{n,j} > h_{n,k}}} p_{n,j} + |\sigma_n|^2} \right) \\ &= \sum_{i=1}^K BW_n \log_2 \left(1 + \frac{|h_{n,\pi(i)}|^2 p_{n,\pi(i)}}{|h_{n,\pi(i)}|^2 \sum_{j=i+1}^K p_{n,\pi(j)} + |\sigma_n|^2} \right). \end{aligned} \quad (68)$$

Let $\Theta_{n,i} = \sum_{j=i}^K p_{n,\pi(j)}$, $\Theta_{n,i+1} = \sum_{j=i+1}^K p_{n,\pi(j)}$ and $\Theta_{n,K+1} = 0$. Then R_n given in (68) can be rewritten as

$$\begin{aligned} R_n &= \sum_{i=1}^K BW_n \log_2 \left(\frac{|h_{n,\pi(i)}|^2 \Theta_{n,i} + |\sigma_n|^2}{|h_{n,\pi(i)}|^2 \Theta_{n,i+1} + |\sigma_n|^2} \right) \\ &= BW_n \sum_{i=1}^K \log_2 (|h_{n,\pi(i)}|^2 \Theta_{n,i} + |\sigma_n|^2) \\ &\quad - BW_n \sum_{i=1}^K \log_2 (|h_{n,\pi(i)}|^2 \Theta_{n,i+1} + |\sigma_n|^2). \end{aligned} \quad (69)$$

Firstly, we analyze the first-order derivative of R_n with regard to $p_{n,\pi(i)}$ in different cases.

Case 1: $i = 1$. In this case, the k -th MU ($k = \pi(i)$) will decode information before any other MUs and thus the corresponding power allocation $p_{n,\pi(i)}$ does not cause interference to other MUs on the n -th subcarrier. Therefore, the first-order derivative of R_n about $p_{n,\pi(i)}$ is given by

$$\frac{\partial R_n}{\partial p_{n,\pi(i)}} = \frac{BW_n}{\ln 2} \cdot \frac{|h_{n,\pi(1)}|^2}{|h_{n,\pi(1)}|^2 \Theta_{n,1} + |\sigma_n|^2}. \quad (70)$$

Case 2: $2 \leq i \leq K$. In this case, the relevant power allocation $p_{n,\pi(i)}$ will bring interference to MUs which decode information before the k -th MU ($k = \pi(i)$). Thus, the first-order derivative of R_n about $p_{n,\pi(i)}$ can be calculated by (71) on the top of the next page. It is evident that the first-order derivative (70) in *Case 1* is a special case of (71) in *Case 2*. Hence, the first-order derivative of R_n about $p_{n,k}$ can be uniformly expressed as (71).

Additionally, the second-order derivative of R_n can be given by (72) on the top of this page, in which $j = \min\{i, l\}$. Let $H_i^{(n)} = \frac{\partial^2 R_n}{\partial p_{n,\pi(i)}^2}$ and $H_{i,l}^{(n)} = \frac{\partial^2 R_n}{\partial p_{n,\pi(i)} \partial p_{n,\pi(l)}}$. According to

$$\frac{\partial^2 R_n}{\partial \rho_k^2} = -\frac{BW_n}{\ln 2} \cdot \frac{A_{n,k} C_{n,k} (2(A_{n,k} + B_{n,k}) B_{n,k} \rho_k + 2B_{n,k} C_{n,k} + A_{n,k} C_{n,k})}{[(A_{n,k} \rho_k + B_{n,k} \rho_k + C_{n,k})(B_{n,k} \rho_k + C_{n,k})]^2}, \quad (63)$$

$$\frac{\partial^2 R_n}{\partial \rho_m \partial \rho_n} = 0 \quad (m \neq n). \quad (64)$$

$$\begin{aligned} \frac{\partial R_n}{\partial p_{n,\pi(i)}} &= \frac{BW_n}{\ln 2} \cdot \left(\sum_{i'=1}^i \frac{|h_{n,\pi(i')}|^2}{|h_{n,\pi(i')}|^2 \Theta_{n,\pi(i')} + |\sigma_n|^2} - \sum_{i'=1}^{i-1} \frac{|h_{n,\pi(i')}|^2}{|h_{n,\pi(i')}|^2 \Theta_{n,\pi(i'+1)} + |\sigma_n|^2} \right) \\ &= \frac{BW_n}{\ln 2} \cdot \left(\frac{|h_{n,\pi(1)}|^2}{|h_{n,\pi(1)}|^2 \Theta_{n,\pi(1)} + |\sigma_n|^2} + \sum_{i'=2}^i \left(\frac{|h_{n,\pi(i')}|^2}{|h_{n,\pi(i')}|^2 \Theta_{n,\pi(i')} + |\sigma_n|^2} - \frac{|h_{n,\pi(i'-1)}|^2}{|h_{n,\pi(i'-1)}|^2 \Theta_{n,\pi(i')} + |\sigma_n|^2} \right) \right). \end{aligned} \quad (71)$$

$$\begin{aligned} \frac{\partial^2 R_n}{\partial p_{n,\pi(i)} \partial p_{n,\pi(l)}} &= -\frac{BW_n}{\ln 2} \cdot \frac{|h_{n,\pi(1)}|^4}{(|h_{n,\pi(1)}|^2 \Theta_{n,\pi(1)} + |\sigma_n|^2)^2} \\ &\quad - \frac{BW_n}{\ln 2} \cdot \sum_{i'=2}^j \left(\frac{|h_{n,\pi(i')}|^4}{(|h_{n,\pi(i')}|^2 \Theta_{n,\pi(i')} + |\sigma_n|^2)^2} - \frac{|h_{n,\pi(i'-1)}|^4}{(|h_{n,\pi(i'-1)}|^2 \Theta_{n,\pi(i')} + |\sigma_n|^2)^2} \right). \end{aligned} \quad (72)$$

(72), it is clearly that

$$H_{i,l}^{(n)} = \begin{cases} H_i^{(n)}, & i \leq l; \\ H_l^{(n)}, & \text{otherwise.} \end{cases} \quad (73)$$

Therefore, the Hessian matrix of R_n on \mathbf{p}_n can be expressed as

$$\mathbf{H}^{(n)} = \begin{bmatrix} H_1^{(n)} & H_1^{(n)} & \cdots & H_1^{(n)} \\ H_1^{(n)} & H_2^{(n)} & \cdots & H_2^{(n)} \\ \vdots & \vdots & \ddots & \vdots \\ H_1^{(n)} & H_2^{(n)} & \cdots & H_K^{(n)} \end{bmatrix}. \quad (74)$$

Secondly, if $n \neq m$, it is obvious that the first-order and the second-order derivative of R_n with regard to $p_{m,\pi(i)}$ are equal to 0, which is given as

$$\frac{\partial R_n}{\partial p_{m,\pi(i)}} = 0, \quad (75)$$

$$\frac{\partial^2 R_n}{\partial p_{m,\pi(i)} \partial p_{m,\pi(l)}} = 0. \quad (76)$$

In summary, the Hessian matrix of R_n with respect to \mathbf{p} is expressed as

$$\mathbf{H}^{\{\mathbf{p}\}} = \begin{pmatrix} \mathbf{H}^{(1)} & \mathbf{0} & \cdots & \mathbf{0} \\ \mathbf{0} & \mathbf{H}^{(2)} & \cdots & \mathbf{0} \\ \vdots & \vdots & \ddots & \vdots \\ \mathbf{0} & \mathbf{0} & \cdots & \mathbf{H}^{(N)} \end{pmatrix}. \quad (77)$$

Define the negative matrix of $\mathbf{H}^{\{\mathbf{p}\}}$ as $\mathbf{Q}^{\{\mathbf{p}\}} = -\mathbf{H}^{\{\mathbf{p}\}}$. Then the principal minor of the matrix $\mathbf{Q}^{\{\mathbf{p}\}}$ is given as follows:

Case 1: $1 \leq m \leq K$. In this case, we have

$$\begin{aligned} |Q_m^{\{\mathbf{p}\}}| &= \begin{vmatrix} -H_1^{(1)} & -H_1^{(1)} & \cdots & -H_1^{(1)} \\ -H_1^{(1)} & -H_2^{(1)} & \cdots & -H_2^{(1)} \\ \vdots & \vdots & \ddots & \vdots \\ -H_1^{(1)} & -H_2^{(1)} & \cdots & -H_m^{(1)} \end{vmatrix} \\ &= \begin{vmatrix} -H_1^{(1)} & -H_1^{(1)} & \cdots & -H_1^{(1)} \\ 0 & H_1^{(1)} - H_2^{(1)} & \cdots & H_1^{(1)} - H_2^{(1)} \\ \vdots & \vdots & \ddots & \vdots \\ 0 & 0 & \cdots & H_{m-1}^{(1)} - H_m^{(1)} \end{vmatrix} \\ &= \begin{cases} -H_1^{(1)}, & m = 1; \\ -H_1^{(1)} \prod_{m'=2}^m (H_{m'-1}^{(1)} - H_{m'}^{(1)}), & 2 \leq m \leq K. \end{cases} \end{aligned} \quad (78)$$

According to (72), it can be easily inferred that

$$-H_1^{(1)} = \frac{BW_1}{\ln 2} \cdot \frac{|h_{1,\pi(1)}|^4}{(|h_{1,\pi(1)}|^2 \Theta_{1,\pi(1)} + |\sigma_1|^2)^2}, \quad (79)$$

which is always non-negative.

Besides, we have

$$\begin{aligned} H_{m'-1}^{(1)} - H_{m'}^{(1)} &= \frac{BW_1}{\ln 2} \cdot \frac{|h_{1,\pi(m')}|^4}{(|h_{1,\pi(m')}|^2 \Theta_{1,\pi(m')} + |\sigma_1|^2)^2} \\ &\quad - \frac{BW_1}{\ln 2} \cdot \frac{|h_{1,\pi(m'-1)}|^4}{(|h_{1,\pi(m'-1)}|^2 \Theta_{1,\pi(m')} + |\sigma_1|^2)^2}. \end{aligned} \quad (80)$$

Since $\tilde{h}_{1,\pi(m')} > \tilde{h}_{1,\pi(m'-1)}$ and accordingly $|h_{1,\pi(m')}|^2 > |h_{1,\pi(m'-1)}|^2$, it can be inferred that $H_{m'-1}^{(1)} - H_{m'}^{(1)} \geq 0$ always holds.

Case 2: $K < \tilde{m} \leq NK$. In this case, we have

$$\begin{aligned}
|Q_m^{\{p\}}| &= \begin{vmatrix} -\mathbf{H}^{(1)} & \cdots & \mathbf{0} & \mathbf{0} \\ \vdots & \ddots & \vdots & \vdots \\ \mathbf{0} & \cdots & -\mathbf{H}^{(\tilde{n})} & \mathbf{0} \\ \mathbf{0} & \cdots & \mathbf{0} & Q_m^{\{p\}} \end{vmatrix} \quad (81) \\
&= |Q_m^{\{p\}}| \cdot \prod_{\tilde{n}'=1}^{\tilde{n}} (|-\mathbf{H}^{(\tilde{n}')}|),
\end{aligned}$$

where $\tilde{m} = \tilde{n}K + m$ ($1 \leq m \leq K$). Actually, we have $|-\mathbf{H}^{(1)}| = \prod_{m=K}^{\tilde{n}} |Q_m^{\{p\}}|$, and hence it is non-negative. Similarly, $|-\mathbf{H}^{(\tilde{n})}| \geq 0$.

Therefore, any principal minor of the matrix $\mathbf{Q}^{\{p\}}$ is non-negative, which implies that $\mathbf{Q}^{\{p\}} \succeq \mathbf{0}$ and $\mathbf{H}^{\{p\}} \preceq \mathbf{0}$. Consequently, R_n is concave with respect to \mathbf{p} . And R_{sum} is also concave on \mathbf{p} due to the fact that the sum of a finite number of concave functions remains concave. This completes the proof of *Proposition 3*. ■

REFERENCES

- [1] C. Bockelmann, N. Pratas, H. Nikopour, K. Au, T. Svensson, C. Stefanovic, P. Popovski, and A. Dekorsy, "Massive machine-type communications in 5G: physical and MAC-layer solutions," *IEEE Commun. Mag.*, vol. 54, no. 9, pp. 59–65, Sep. 2016.
- [2] Z. Ding, X. Lei, G. K. Karagiannidis, R. Schober, J. Yuan, and V. K. Bhargava, "A survey on non-orthogonal multiple access for 5G networks: Research challenges and future trends," *IEEE J. Sel. Areas Commun.*, vol. 35, no. 10, pp. 2181–2195, Oct 2017.
- [3] L. Dai, B. Wang, Z. Ding, Z. Wang, S. Chen, and L. Hanzo, "A survey of non-orthogonal multiple access for 5G," *IEEE Commun. Surveys Tut.*, vol. 20, no. 3, pp. 2294–2323, thirdquarter 2018.
- [4] T. Cover, "Broadcast channels," *IEEE Trans. Info. Theory*, vol. 18, no. 1, pp. 2–14, January 1972.
- [5] A. Benjebbour, Y. Saito, Y. Kishiyama, A. Li, A. Harada, and T. Nakamura, "Concept and practical considerations of non-orthogonal multiple access (NOMA) for future radio access," in *Proc. IEEE Intell. Signal Process. and Commun. Syst. (IEEE ISPACS)*, Nov 2013, pp. 770–774.
- [6] Z. Ding, Z. Yang, P. Fan, and H. V. Poor, "On the performance of non-orthogonal multiple access in 5G systems with randomly deployed users," *IEEE Signal Process. Lett.*, vol. 21, no. 12, pp. 1501–1505, Dec 2014.
- [7] Y. Saito, A. Benjebbour, Y. Kishiyama, and T. Nakamura, "System-level performance of downlink non-orthogonal multiple access (NOMA) under various environments," in *Proc. IEEE Veh. Tech. Conf. (IEEE VTC Spring)*, May 2015, pp. 1–5.
- [8] F. Alavi, K. Cumanan, Z. Ding, and A. G. Burr, "Beamforming techniques for nonorthogonal multiple access in 5G cellular networks," *IEEE Trans. Veh. Tech.*, vol. 67, no. 10, pp. 9474–9487, Oct 2018.
- [9] —, "Robust beamforming techniques for non-orthogonal multiple access systems with bounded channel uncertainties," *IEEE Commun. Lett.*, vol. 21, no. 9, pp. 2033–2036, Sep. 2017.
- [10] Z. Ding, F. Adachi, and H. V. Poor, "The application of MIMO to non-orthogonal multiple access," *IEEE Trans. Wireless Commun.*, vol. 15, no. 1, pp. 537–552, Jan 2016.
- [11] Y. Liu, Z. Ding, M. ElKashlan, and J. Yuan, "Nonorthogonal multiple access in large-scale underlay cognitive radio networks," *IEEE Trans. Veh. Tech.*, vol. 65, no. 12, pp. 10152–10157, Dec 2016.
- [12] Z. Ding, M. Peng, and H. V. Poor, "Cooperative non-orthogonal multiple access in 5G systems," *IEEE Commun. Lett.*, vol. 19, no. 8, pp. 1462–1465, Aug 2015.
- [13] M. Alkhawtrah, Y. Gong, G. Chen, S. Lambotharan, and J. A. Chambers, "Buffer-aided relay selection for cooperative noma in the internet of things," *IEEE Internet of Things Journal*, vol. 6, no. 3, pp. 5722–5731, June 2019.
- [14] X. Lu, P. Wang, D. Niyato, D. I. Kim, and Z. Han, "Wireless networks with RF energy harvesting: A contemporary survey," *IEEE Commun. Surveys Tut.*, vol. 17, no. 2, pp. 757–789, Secondquarter 2015.
- [15] L. R. Varshney, "Transporting information and energy simultaneously," in *Proc. IEEE ISIT*, July 2008, pp. 1612–1616.
- [16] X. Zhou, R. Zhang, and C. K. Ho, "Wireless information and power transfer: Architecture design and rate-energy tradeoff," *IEEE Trans. Commun.*, vol. 61, no. 11, pp. 4754–4767, November 2013.
- [17] G. Chen, P. Xiao, J. R. Kelly, B. Li, and R. Tafazolli, "Full-duplex wireless-powered relay in two way cooperative networks," *IEEE Access*, vol. 5, pp. 1548–1558, 2017.
- [18] L. Liu, R. Zhang, and K. Chua, "Wireless information and power transfer: A dynamic power splitting approach," *IEEE Trans. Commun.*, vol. 61, no. 9, pp. 3990–4001, Sep. 2013.
- [19] Q. Shi, L. Liu, W. Xu, and R. Zhang, "Joint transmit beamforming and receive power splitting for MISO SWIPT systems," *IEEE Trans. Wireless Commun.*, vol. 13, no. 6, pp. 3269–3280, June 2014.
- [20] J. Tang, D. K. C. So, N. Zhao, A. Shojaefard, and K. Wong, "Energy efficiency optimization with SWIPT in MIMO broadcast channels for Internet of Things," *IEEE Internet Things J.*, vol. 5, no. 4, pp. 2605–2619, Aug 2018.
- [21] X. Zhou, R. Zhang, and C. K. Ho, "Wireless information and power transfer in multiuser OFDM systems," *IEEE Trans. Wireless Commun.*, vol. 13, no. 4, pp. 2282–2294, April 2014.
- [22] J. Tang, J. Luo, M. Liu, D. K. C. So, E. Alsusa, G. Chen, K. Wong, and J. A. Chambers, "Energy efficiency optimization for NOMA with SWIPT," *IEEE J. Sel. Topics Signal Process.*, vol. 13, no. 3, pp. 452–466, June 2019.
- [23] Y. Xu, C. Shen, Z. Ding, X. Sun, S. Yan, G. Zhu, and Z. Zhong, "Joint beamforming and power-splitting control in downlink cooperative SWIPT NOMA systems," *IEEE Trans. Signal Process.*, vol. 65, no. 18, pp. 4874–4886, Sep. 2017.
- [24] M. Hedayati and I. Kim, "On the performance of NOMA in the two-user SWIPT system," *IEEE Trans. Veh. Tech.*, vol. 67, no. 11, pp. 11258–11263, Nov 2018.
- [25] Y. Sun, D. W. K. Ng, Z. Ding, and R. Schober, "Optimal joint power and subcarrier allocation for full-duplex multicarrier non-orthogonal multiple access systems," *IEEE Trans. Commun.*, vol. 65, no. 3, pp. 1077–1091, March 2017.
- [26] B. Mao, Z. M. Fadlullah, F. Tang, N. Kato, O. Akashi, T. Inoue, and K. Mizutani, "Routing or computing? The paradigm shift towards intelligent computer network packet transmission based on deep learning," *IEEE Trans. Comput.*, vol. 66, no. 11, pp. 1946–1960, Nov 2017.
- [27] L. Ghouti, "Mobility prediction using fully-complex extreme learning machines," in *Proc. 22nd European Symposium on Artificial Neural Networks, Computational Intelligence and Machine Learning*, 2014, pp. 607–612.
- [28] B. Bojovic, E. Meshkova, N. Baldo, J. Riihijarvi, and M. Petrova, "Machine learning-based dynamic frequency and bandwidth allocation in self-organized LTE dense small cell deployments," *EURASIP J. Wireless Commun. Net.*, vol. 2016, 12 2016.
- [29] Y. Fu, L. Salan, C. W. Sung, and C. S. Chen, "Subcarrier and power allocation for the downlink of multicarrier NOMA systems," *IEEE Trans. Veh. Tech.*, vol. 67, no. 12, pp. 11833–11847, Dec 2018.
- [30] K. Singh, K. Wang, S. Biswas, Z. Ding, F. A. Khan, and T. Ratnarajah, "Resource optimization in full duplex non-orthogonal multiple access systems," *IEEE Trans. Wireless Commun.*, vol. 18, no. 9, pp. 4312–4325, Sep. 2019.
- [31] S. Boyd and L. Vandenberghe, *Convex Optimization*. Cambridge University Press, Cambridge, UK, 2004.
- [32] L. Zhang, Y. Xin, and Y. Liang, "Weighted sum rate optimization for cognitive radio MIMO broadcast channels," *IEEE Trans. Wireless Commun.*, vol. 8, no. 6, pp. 2950–2959, June 2009.
- [33] J. J. M. Paul H. Calamai, "Projected gradient methods for linearly constrained problems," *Mathematical Programming*, vol. 39, no. 1, pp. 93–116, 1987.
- [34] X. Cao, R. Ma, L. Liu, H. Shi, Y. Cheng, and C. Sun, "A machine learning-based algorithm for joint scheduling and power control in wireless networks," *IEEE Internet Things J.*, vol. 5, no. 6, pp. 4308–4318, Dec 2018.
- [35] GreenTouch, *Mobile Communications WG architecture doc2: Reference scenarios*, May. 2013.
- [36] D. W. K. Ng, E. S. Lo, and R. Schober, "Wireless information and power transfer: Energy efficiency optimization in OFDMA systems," *IEEE Trans. Wireless Commun.*, vol. 12, no. 12, pp. 6352–6370, December 2013.
- [37] T. N. Do and B. An, "Optimal sum-throughput analysis for downlink cooperative SWIPT NOMA systems," in *Proc. International Conference Recent Advances in Signal Processing, Telecommunications Computing (SigTelCom)*, Jan 2018, pp. 85–90.
- [38] J. Luo, J. Tang, D. K. C. So, G. Chen, K. Cumanan, and J. A. Chambers, "A deep learning-based approach to power minimization in multi-carrier NOMA with SWIPT," *IEEE Access*, vol. 7, pp. 17450–17460, 2019.